Journal of Engineering Science and Technology
Special Issue on SU18, February (2019) 179 - 190
© School of Engineering, Taylor's University

PERFORMANCE ANALYSIS OF COGGING TORQUE REDUCTION TECHNIQUE ON HYBRID FLUX SWITCHING MOTOR

JAUDAH ABD RANI*, ERWAN SULAIMAN

Faculty of Electrical and Electronics Engineering, Universiti Tun Hussein Onn Malaysia, 86400 Parit Raja, Batu Pahat, Johor, Malaysia
*Corresponding Author: he150066@siswa.uthm.edu.my

Abstract

The structural nature of Hybrid Flux Switching Motor (HFSM) is a high-performance motor with powerful output torque. However, the air-gap flux density causes the motor to suffer noise and vibration at the low operating region. In this paper, an E-Core HFSM undergoes cogging torque reduction techniques in the discussion. The technique being employed are notching and chamfering on the rotor pole. The analysis carried out from the rotor-pole stage study, which established the initial design. Then from the initial design, the design undergoes optimization on the rotor pole with the objective to achieve lower cogging torque than the initial design.

Keywords: Chamfering, Cogging torque, Hybrid flux switching motor, Notching.

1. Introduction

Cogging torque comes from the interaction between the rotor part, which commandeer the motor rotational motion. Meanwhile, the stator part, which is the stationary part. In addition, it is compulsory for the existence of the permanent magnet in either side of the motor to rationalize the concept of flux switching motor. Cogging torque emerges because the permanent magnet, neither being position in the stator or the rotor, will have the tendency to align with the iron. The iron being said could be the stator or the rotor [1].

In the past, a study on a number of rotor and stator combination that best fit for E-Core HFSM had been studied. It was found that 10P-4S rotor pole and stator pole combination had the best fit. This paper will focus on the performance analysis on which, the cogging torque reduction technique will take place on the rotor structure. The study will extensively compare the load and no-load analysis between the initial design and the design that undergoes cogging torque reduction technique to achieve optimum performance with minimal cogging torque.

From the past research, the effect of cogging torque reduction technique implicated different effect on every geometrical design it was implied. In each motor, it has different geometrical design restricted by the size, operating principles, and operating supply. Although all the technique is the same, the employment on the design changes the structure of the motor that in turn change the output performance of the motor.

2. Cogging Torque

In general, the cogging torque reduction technique can be divided into two methods. Firstly, the control method on which, involve designing a controller to control the injected current in terms of its magnitude and frequency as well as the phase. Such a method mostly covers control design such as harmonic-current-injection based active control schemes [1].

Secondly, the design method where the researcher devises every part of the motor such as the rotor and the stator. In devising the design, multiple techniques were produced, which were proven to successfully reduce the cogging torque in the output torque production. The torque ripple contributes the cogging torque. Therefore, the reduction technique is to study the torque ripple suppression strategy in order to stabilize the torque component of the motor. The torque ripple may result from flux harmonic, reluctance torque, and cogging torque, deviation in measuring current and asymmetric motor structure [1].

The said techniques are skewing, permanent magnet shift, pole pairing, notching, and chamfer. Skewing can reduce cogging torque effectively. Fei et al. [2] explained that an optimal pole step-skew method is proposed. However, it is not easy to achieve in the manufacturing process. Furthermore, it would make the motor structure more complex. First, skewing is widely used to reduce torque ripple [3-5], in which, the stator slots or rotor poles are skewed to reduce the cogging torque. However, the skewed stator or rotor is harder to build for manufacturing, which also increases the cost of production. Then, the auxiliary slots or teeth are used to replace the skewing to avoid the disadvantages from skewing at the loss of efficiency [6], current and asymmetric motor structure [7, 8].

Fei et al. [5] reported that a shifting PM method is presented to solve the problem of magnetic pole modelling, a modified subdomain model method based on the discrete idea is proposed to predict magnetic field distribution in the air-gap. Meanwhile, the uniform analytical expressions of cogging torque with shifting PMs are established. However, the calculation will be more complex when there are more poles.

The cogging torque will be influenced by adjusting the air-gap permeance and the distribution of the air-gap flux density. Xu et al. [9] presented two types of eccentric magnetic pole shapes for optimizing PM synchronous machines with radial magnetization. An analytical method based on an exact subdomain is also proposed for calculating the air-gap flux density distribution in the optimized motor.

The design method proved to have significant to the cogging torque in the said literature remarkably reduced. The said technique proposed able to achieve the goal of reducing the cogging torque.

3. Performance of E-Core HFSM

Initially, the rotor-pole combination was studied and the topologies are illustrated in Fig. 1. The average torque and output power obtained were the base value obtained on which, were believed could be improved further. From Fig. 1, 4S-10P rotor pole configuration excited the average torque and output power. The design was optimized by refining the parameters defined in Fig. 2 using the design of experiment technique by updating each parameter with respect to the electrical design parameter of the motor defined in Table 1.

The first step is conducted by changing rotor parameters, P_1, P_2, and P_3. As P_1 represents the radius of the rotor and it has a major effect on torque enhancement, thus, R_1 is firstly updated. At this stage, the magnet parameters P_4 and P_5 are also adjusted with the following P_1 to ensure constant magnet volume in the stator. The torque is maximized when P_1, P_2, and P_3 are set to 94.5 mm, 36 mm, and 10.55 mm, respectively as illustrated in Table 2. The refining procedure is carried on by updating field excitation slot area, such that circumferential radius from the centre point, P_9, and width, P_8 while the previous design parameters are kept invariable. When P_9 and P_8 are 118.37 mm and 26 mm, correspondingly, the maximum torque is obtained. Then, by using the optimum combination of P_9 and P_8 the armature coil slot parameters, P_6 and P_7 are varied. The essential armature coil slot area, S_a is determined by altering armature coil depth, P_6 and P_7 to provide enough space for a natural number of turns of armature coil.

Table 2 shows the comparison between the geometrical parameter define during the rotor-pole study and after the refining process as well as the performance output of the motor. The geometrical parameter and performance output established after the refining process make up the initial condition of the motor on which, believed able to be improved further upon reduction of cogging torque.

It is observed that the torque increase from 183.6 Nm to 243.14 Nm an increase of 32% and power increase up to 71.18% from 32.72 kW to 36.72 kW. The initial performance of the motor is powerful for a single phase motor. However, it has two drawbacks that are the cogging torque and the distorted back emf. The initial design in Fig. 3 register cogging torque of 108.45 Nm, comparing the design at the rotor-pole study in Fig. 1, the cogging torque is 50.87 Nm. For a powerful motor to operate smoothly with minimal noise and vibration the cogging torque is viable at less than

10% from its output torque. Besides, the cogging torque is directly influenced by the electromotive force of the motor. Since the cogging torque, heavily influence the motor electromotive force, a high cogging torque will influence a high back emf.

The back emf of the initial design is at 0.3 V comparing at the rotor-pole design stage, which is at 0.2 V. The back emf should be less than the applied voltage to ensure the motor is operating at safe operating region without damaging the coil. The comparison of the back emf is illustrated in Fig. 4. Evidently, the leakage flux to the surrounding area in the design at the rotor stage has been mitigated by the initial design. Besides, a large amount of flux contributed by the magnet in the initial proposed design is cancelled by flux from the field excitation coil. In reality, the stator teeth thickness and stator core in the initial design has been expanded, allowing the flux to flow easily and enhanced the machine performances. The behaviour of flux linkages in initial and optimized designs are obtained by the following Eq. (1).

$$\phi_g = \int_0^{\frac{\pi}{p}} B_g \sin(p\theta_s - (\omega_m t + \theta_0) l_s r_s d\theta_s \quad (1)$$

where B_g is the air gap magnetic flux density, ls is stator length, r_s is the radius at middle air gap, Θ_s is the mechanical angle along stator edge, ω_m is the rotor angular speed and Θ_0 is the rotor initial position.

Table 1. Electrical parameter restriction.

Electrical parameters	Value
Maximum DC voltage (V)	230
Maximum armature current (A_{rms})	360
Maximum armature current density, J_a (A_{rms}/mm^2)	30
Maximum field current density, J_e (A/mm^2)	30
Volume of PM (kg)	1.3
Maximum average torque (Nm)	183
Maximum output power (kW)	36
Power density (kW/kg)	> 1.3

Table 2. Geometrical parameter comparison at rotor-pole design and initial design.

Geometrical parameter	Rotor-pole	Initial
P1 (mm)	85	94.5
P2 (mm)	30	36
P3 (mm)	7.92	10.55
P4 (mm)	6.6553	8.378
P5 (mm)	46.2	36.7
P6 (mm)	0	21
P7 (mm)	118.8	118.9
P8 (mm)	0	26
P9 (mm)	118.8	118.37
Armature slot area (mm^2)	872.40	554.84
Armature number of turns	36	23
PM weight (kg)	1.3	1.3
Average torque (Nm)	183.6	243.14
Airgap (mm)	0.8	0.8
Power (kW)	36.72	62.86
Field excitation slot area (mm^2)	901.54	590.08
Field excitation number of turns	270	177
Speed (rpm)	1914.44	2468.88

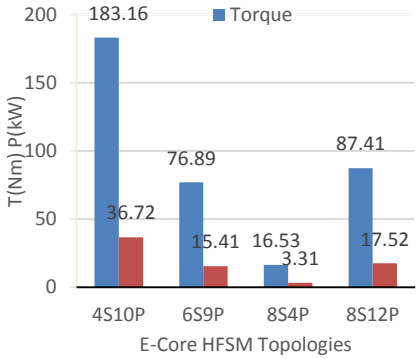

Fig. 1. Performance output of HFSM at rotor-pole design stage.

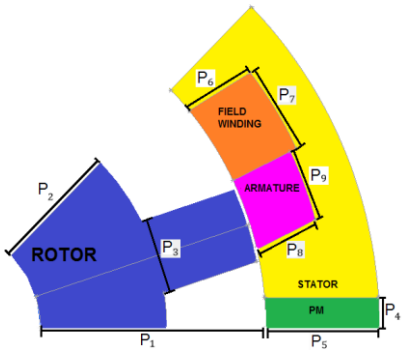

Fig. 2. Initial design parameter of HFSM.

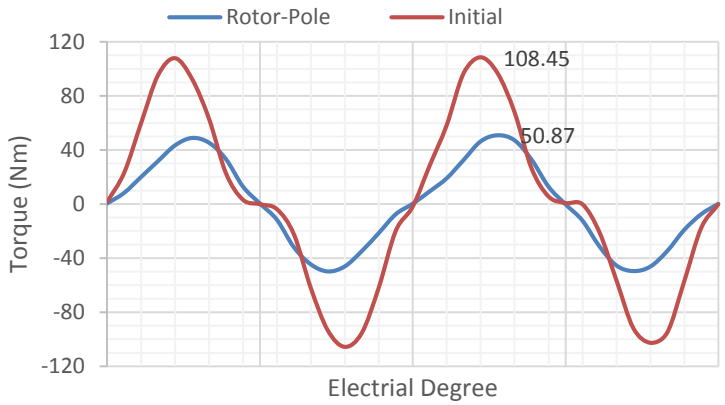

Fig. 3. Cogging torque comparison between design at rotor-pole design stage and initial stage.

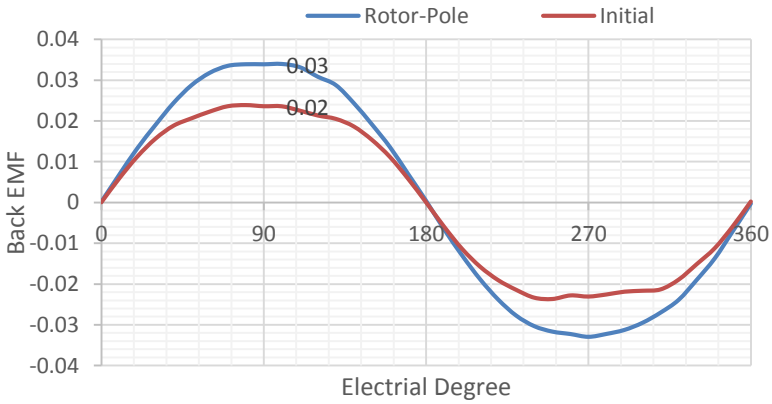

Fig. 4. Back emf comparison between design at rotor-pole design stage and initial stage.

4. Results and Discussion

The cogging torque reduction, which going to be implemented on the initial design is notching, pole pairing and chamfering. The three cogging torque reduction techniques mentioned earlier had been identified justified given the circumstances that it is implemented on the design factor without compromising the major structure of the motor. Therefore, all three techniques will be applicable on the rotor side of the motor. It is important for the motor to maintain the initial design because altering the motor structure that can be achieved through skewing may affect the average torque and output power of the motor that the least prospect of the result to be achieved.

In HFSM, under no load condition, the torque acting on each stator teeth can be defined as

$$T_{single}(\theta) = \sum_{n=1}^{\infty} T_n \sin(nN_r\theta) \quad (2)$$

where T_n, is the amplitude of the torque with respect to the n^{th} harmonic and θ rotor pole position. From Eq. (1), the cogging torque can be calculated by each torque action on the stator teeth as Eq. (3) in which, it can deduce the cogging torque can be reduced by lowering the T_n through changing the rotor design.

$$T(\theta) = \sum_{n=1}^{\infty} \left\{ T_n \, sin(nN_r\theta) \sum_{k=0}^{N_s-1} \left[cos \, 2\pi k \frac{nN_r}{N_s} \right] \right\} \quad (3)$$

4.1. Notching

According to Saadha et al. [10], notching technique is when a dip is introduced to the outer surface of the rotor pole with similar work done in the literature for linear applications. It may compromise the back emf and magnitude of the cogging torque due to the enlargement of the air-gap between the rotor and the stator teeth. The configuration of the notch can be divided into two, which are a number of the notch and the notch dimension.

The proposed notching technique can be observed in Fig. 5, where Fig. 5(a) shows the dimensional consideration of the notch consists of the height (h) and the notch length (l). Figure 5(b) shows the number of the notch to be an experiment for the configuration. Both notch dimension and number of the notch is analysed differently in two separate analysis.

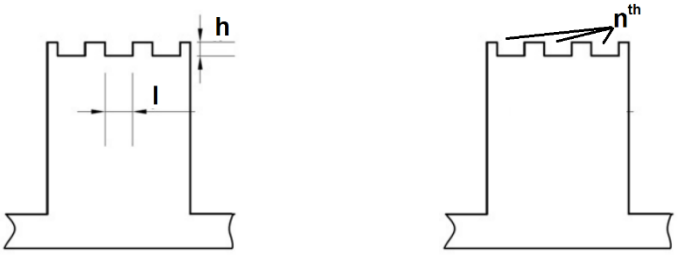

Fig. 5. Cogging torque reduction technique of notching.

Figure 6 shows the torque component under notch dimension, which comprised of instantaneous torque, average torque, and cogging torque. The instantaneous

torque was recorded under load condition at maximum armature and field excitation current condition, which results in the amplitude of 447.42 Nm with the average torque of 243.14 Nm. Meanwhile the cogging torque register amplitude of 35.27 Nm that is much lower than the initial design cogging torque.

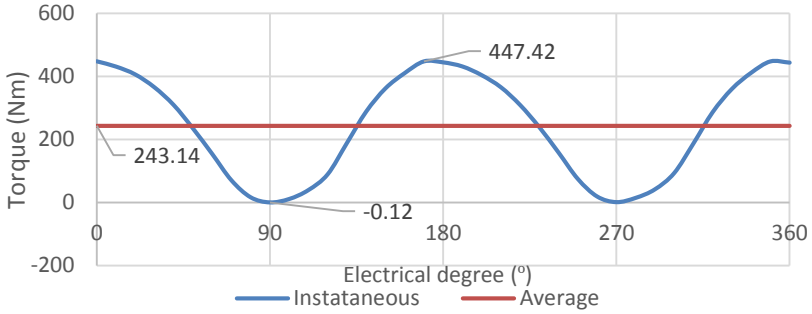

(a) Torque at load condition.

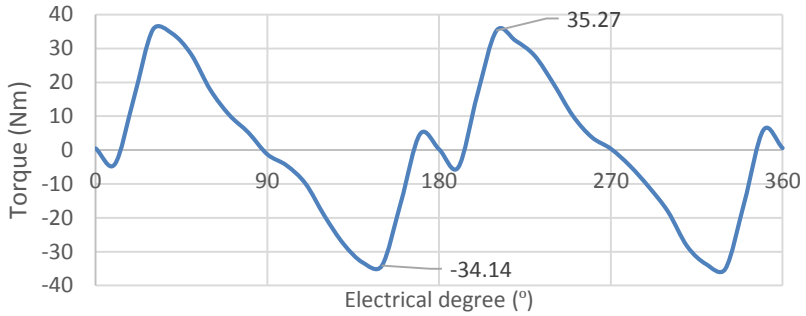

(b) Cogging torque.

Fig. 6. Torque component resulting from dimensional notching.

Figure 7 shows the torque component under a variation number of the notch of one, which comprised of instantaneous torque, average torque, and cogging torque. The instantaneous torque was recorded under load condition at maximum armature and field excitation current condition, which results in the amplitude of 433.66 Nm with the average torque of 237.75 Nm. Meanwhile, the cogging torque register amplitude of 82.72 Nm that is lower than the initial design cogging torque but higher than the cogging torque under dimensional notch. Figure 8 shows the cogging torque decrease from 98 Nm of peak-to-peak cogging torque value with increasing number of the notch with reversing pattern after the 6^{th} notch. However, the constant decrement of stair pattern can be observed on the output torque as it started at 237 Nm on the first notch and going down to 226 Nm on the 10^{th} notch. The minimization of the cogging torque effectively explained by the decreasing air gap flux.

Meanwhile, Fig. 9 shows the magnetic field comparison resulting between the notching of a number of the notch and the dimensional notching. The magnetic field area in Fig. 9(a) is more intense compared to the magnetic field in Fig. 9(b). This may due to the enlargement of air-gap between the rotor-stator and the stator teeth.

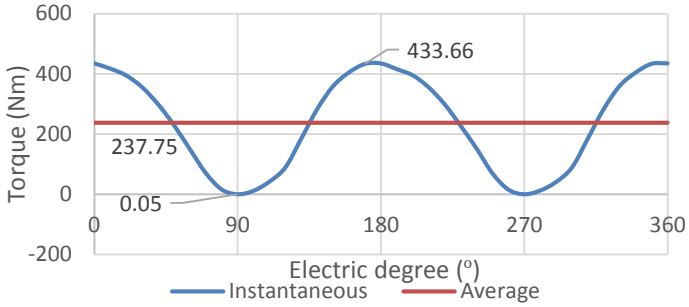

(a) Torque at load condition.

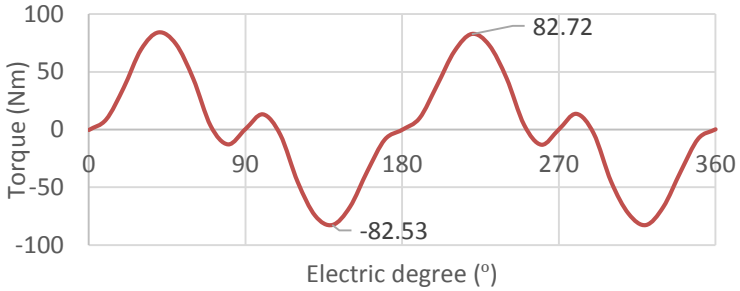

(b) Cogging torque.

Fig. 7. Torque component resulting from number of notch notching.

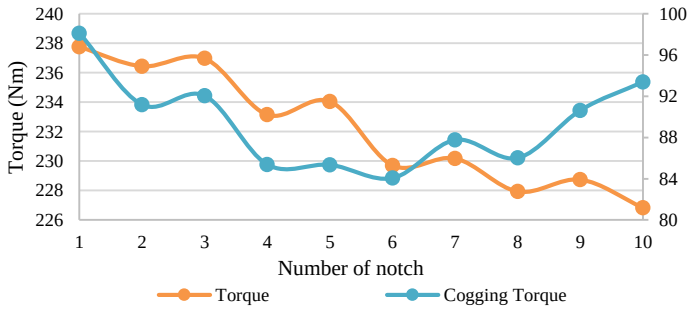

Fig. 8. Influence of notch number on torque and cogging torque.

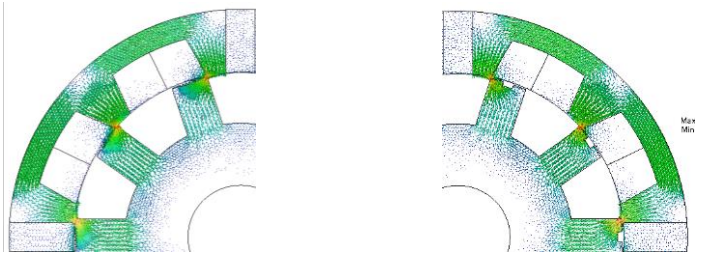

(a) Number of notch. **(b) Dimensional notching.**

Fig. 9. Magnetic field comparison.

4.2. Chamfering

In previous research, chamfering can be divided into two types, which is curve chamfer and right-angle chamfer had been widely implemented for optimization purposes of reducing the cogging torque. The curve and right-angled chamfer implemented on the rotor tooth is as illustrated in Figs. 10(a) and (b), respectively.

The curve chamfer is applied by varying the curve radius represented in Fig. 10(a) from 1 mm up to 5 mm. From the variation, 1 mm of curve radius brought out the highest performance. Meanwhile, the right-angle chamfer is varied by the width of the gradient width, w from 1 mm up to 10 mm. The width gradient of 2 mm expedites the highest performance of the motor. Both of the chamfer technique is evaluated for the initial design with the objective to reduce the cogging torque.

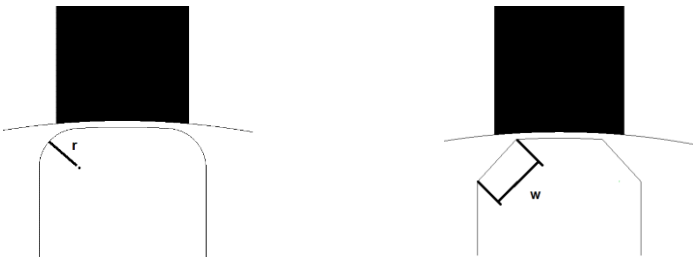

Fig. 10. Cogging torque reduction technique of chamfering.

The Finite-Element Analysis (FEA) ran on the design with curve chamfering is shown in Fig. 11(a) where the peak-to-peak instantaneous torque peaking at 452.18 Nm with the average torque of 242.93 Nm. Correspondingly, the cogging torque is 117.13 Nm as illustrated in Fig. 11(b), which is higher than the initial design. It can be inferred by employing curve chamfer it decreases the average torque and increases the cogging torque.

In a different analysis of FEA with right-angle chamfer, the rotor pole is kept constant from the initial design and the right angle chamfer applied on the rotor pole. At 2 mm of the right-angle chamfer, the performance of the motor is illustrated in Fig. 12(a) where the peak value of the instantaneous torque is 252.32 Nm with the average torque of 242.99 Nm. The cogging torque resulted from right angle chamfer is 121.60 nm, which is higher than the cogging torque from the initial design illustrated in Fig. 12(b).

Figure 13 .shows the magnetic field under both chamfering conditions. It can be seen that with right angle chamfer, the magnetic field is more intense compared to the magnetic field with curve chamfer. This explained the higher cogging torque register with right-angle chamfer due to flux leakage at the yip of the rotor pole. The flux leakage influence the negative torque component, which cancel out the positive torque that contributed to the cogging torque.

The comparison of the torque component of the 4S10P E-Core HFSM from the initial design and the design under the influence of the cogging torque reduction technique is shown in Fig. 14. Generally, the average torque of design with

reduction technique implied is less than the initial design. The same pattern observes with the peak-to-peak value of the instantaneous torque with the design with the reduction technique employed.

However, the cogging torque reduction technique does influence the cogging torque. The dimensional notch has the biggest cogging torque drop from 10.45 Nm to 35.27 Nm. However, both chamfering techniques have the inverse effect of the expected cogging torque where the cogging torque rise from 108.45 Nm to 117.36 Nm and 121.6 Nm for curve chamfer and right angle chamfer, respectively.

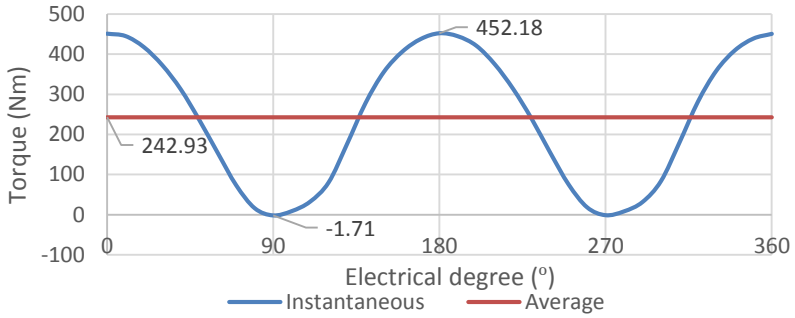

(a) Torque at load condition.

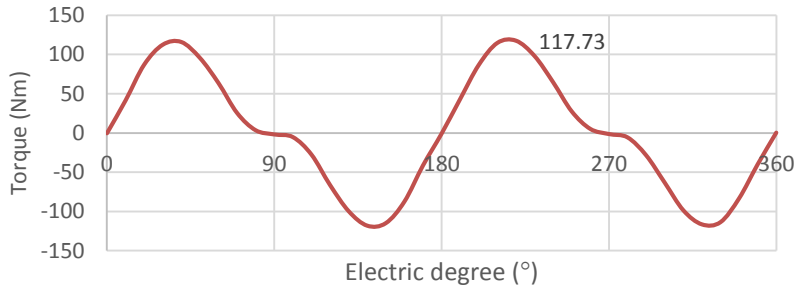

(b) Cogging torque.

Fig. 11. Torque component resulting from number of curve notching.

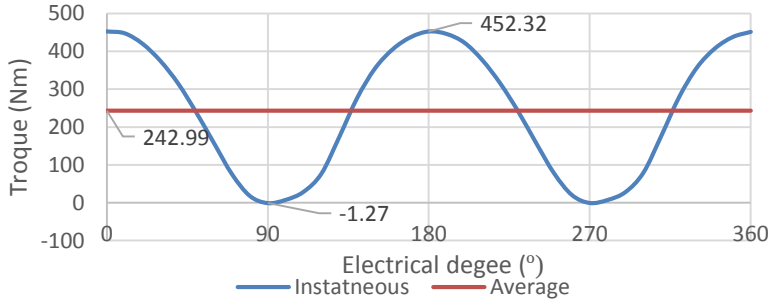

(a) Torque at load condition.

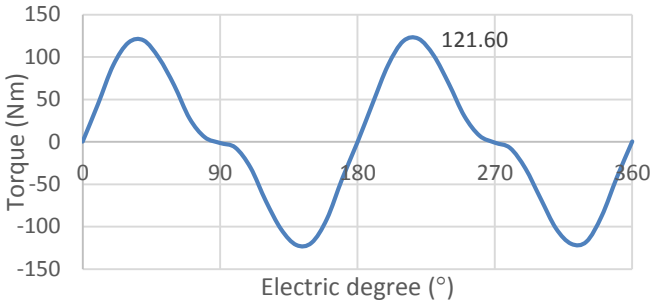

(b) Cogging torque.

Fig. 12. Torque component resulting from number of right angle chamfering.

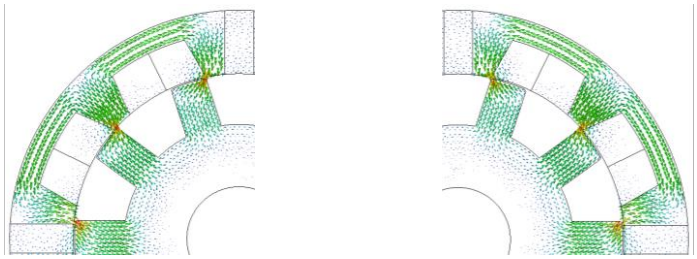

(a) Curve chamfering. **(b) Right angle chamfering.**

Fig. 13. Magnetic field comparison.

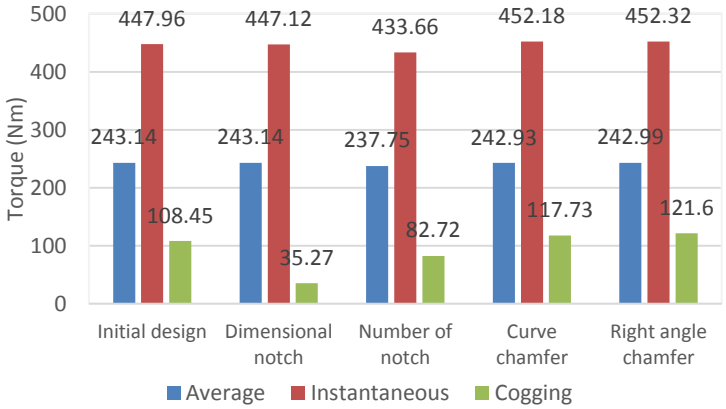

Fig. 14. Torque component comparison of initial design and design influence by reduction technique.

5. Conclusions

In conclusion, the design optimization achieved lower cogging torque. For the design of 4S10P HFSM, the appropriate cogging torque technique is a dimensional notch that results of 67% of cogging torque reduction. However, the cogging torque component of the design with the dimensional notch employment to the output torque is at 14.50%. The best performance for the motor is to have less than 10%

of the cogging torque component to the output torque. Therefore, the design can be further optimized with other technologies in a future study.

Acknowledgement

This research work was funded by the Ministry of Education Malaysia (MoE) under the Fundamental Research Grant Scheme (FRGS), Vot. Number 1651 through Universiti Tun Hussein Onn Malaysia.

References

1. Jia, H.; Cheng, M.; Hua, W.; Zhao, W.; and Li, W. (2010). Torque ripple suppression in flux-switching PM motor by harmonic current injection based on voltage space-vector modulation. *IEEE Transactions on Magnetics*, 46(6), 1527-1530.
2. Fei, W.; Luk, P.C.K.; and Shen, J. (2012). Torque analysis of permanent-magnet flux switching machines with rotor step skewing. *IEEE Transactions on Magnetics*, 48(10), 2664-2673.
3. Bahrim, F.S.; Sulaiman, E.; Jusoh, L.I.; Omar, M.F.; and Kumar, R. (2017). Cogging torque reduction of IPM motor using skewing, notching, pole pairing and rotor pole axial pairing. *International Journal of Applied Engineering Research*, 12(7), 1371-1376.
4. Lazari, P.; Wang, J.; and Sen, B. (2015). 3-D Effects of rotor step-skews in permanent magnet-assisted synchronous reluctance machines. *IEEE Transactions on Magnetics*, 51(11), 1-4.
5. Fei, W.; Luk, P.C.K.; Xia, B.; Wang, Y.; and Shen, J.X. (2010). Permanent magnet flux switching integrated-starter-generator with different rotor configurations for cogging torque and torque ripple mitigations. *IEEE Energy Conversion Congress and Exposition (ECCE)*, 1715-1722.
6. Lindner, A.; and Hahn, I. (2015). Design of an E-core flux-switching permanent magnet machine with large air-gap. *Proceedings of the IEEE International Electric Machines and Drives Conference* (IEMDC). Coeur d'Alene, Idaho, United States of America, 1580-1585.
7. Lindner, A. (2016). Alternative ways of cooling an E-core flux- switching permanent magnet machine with large air-gap. *Proceedings of the 42nd Annual Conference of the IEEE Industrial Electronics Society*. Florence, Italy, 1596-1603.
8. Hu, J.H.; Wang, L.; Zou, J.B.; and Zhao, B. (2016). Cogging torque reduction of hybrid excitation flux switching motor. *Proceedings of the 5th International Conference on Instrumentation and Measurement, Computer, Communication and Control* (IMCCC), 2(5), 1889-1892.
9. Xu, D.; Lin M.; Fu, X.; Hao L.; Zhang, W.; and Li, N. (2016). Cogging torque reduction of a hybrid axial field flux-switching permanent-magnet machine with three methods. *IEEE Transactions on Applied Superconductivity*, 26(24), Article No. 5201305.
10. Saadha, A.; Aravind, C.V.; Krishna, P.; and Azhar, F. (2017). Electromagnetic design analysis of single-layered linear switching machine with fixed DC excitation for rail brake systems. *Proceedings of the 15th Students Conference on Research and Development* (SCOReD). Putrajaya, Malaysia, 371-276.